Supporting Information

Closed Pore Architecture and Sodium Cluster Deposit Visualization in Hard Carbon

Bobo Sun,[1,2‡] Ruohan Yu,[1‡] Yuxia Zhong,[1,2] Jinshuai Liu,[1,2] Zihe Wei,[1,2] Xia Wang,[1,2] Guangwan Zhang,[1,2] Meng Huang,[1] Lei Zhang,[1,2] Qin Wang,[3] Fei Lv,[3] and Liang Zhou,[1,2]*

[1]The Sanya Science and Education Innovation Park, Wuhan University of Technology, Sanya 572000, The People's Republic of China.

[2]State Key Laboratory of Advanced Technology for Materials Synthesis and Processing, Wuhan University of Technology, Wuhan 430070, The People's Republic of China.

[3]Hubei Wanrun New Energy Technology Co., Ltd., 557 Tianma Road, Yunyang Economic Development Zone, Shiyan 442003, The People's Republic of China.

‡These authors contributed equally.

*Corresponding Authors

Email: liangzhou@whut.edu.cn.

KEYWORDS: hard carbon anode; sodium-ion batteries; closed pore; 3D structural reconstruction; sodium cluster

Materials synthesis. In a typical synthesis, resorcinol (2.18 g), sodium hydroxide (0.012 g), and 37 wt% formaldehyde aqueous solution (3 mL) were dissolved in water (300 mL) by stirring at ambient temperature for 12 h, and a water-soluble phenolic resin solution was obtained. Then, Pluronic F127 (0, 1, and 2 g) was added to the solution, followed by stirring for 1 hour. The mixture was then spray-dried under controlled conditions (temperature: 120 ˚C, gas flow rate: 600 L h^{-1}, feed speed: 5%) to obtain phenolic resin/F127 composite powder, designated as PF/F127. Finally, the PF/F127 was pre-sintered at 350 ˚C for 3 h, and then heated to 1400 ˚C for 3 h under Ar.

Material characterization. Fourier transform infrared spectra were collected on a Fourier transform infrared spectrometer (FTIR, Bruker tensor 27). Thermogravimetric (TG) analysis was carried out using a Netzsch STA449F3 integrated thermal analysis instrument (Germany) under Ar atmosphere with a heating rate of 10 ˚C min^{-1}. X-ray diffraction (XRD) was performed on a Rigaku Smart Lab diffractometer (Japan) operating at 30 kV and 10 mA with a Co Kα radiation source (λ = 1.79 Å). Raman spectroscopy was conducted using a Renishaw InVia Reflex Raman microscope with a 532 nm excitation laser. The Brunauer-Emmett-Teller (BET) surface area and pore size distribution were determined by N_2 (77K) and CO_2 (273K) using a BELSORP-max II (USA) analyzer. Small angle X-ray scattering (SAXS) is tested by Xeuss 2.0 (Xenocs, France). X-ray photoelectron spectroscopy (XPS) analysis was performed on an ESCALAB 250 Xi spectrometer. Scanning electron microscopy (SEM) images were obtained using a JEOL JSM-7100F scanning electron microscope at an accelerating voltage of 15 kV. High-resolution transmission electron microscopy (TEM), high-angle annular dark-field scanning TEM (HAADF-

STEM), electron energy-loss spectroscopy (EELS), and electron tomography experiments were performed using a CEOS probe corrected FEI Titan G2 60-300 Themis TEM instrument with an electron accelerating voltage of 300 kV, equipped with a Gatan image filter spectrometer. The probe convergence angle was 17.8 mrad, and the probe current was approximately 45 pA for STEM imaging and EELS acquisition. EELS data was collected using a Gatan Quantum 965 GIF system. 3D reconstruction was performed using Thermo Fisher 3D Inspect and visualized in Avizo software.

Electrochemical analysis. The electrochemical performances were tested by assembling CR2016 coin cells in the Ar-filled glove box. Sodium foil was used as both the counter and reference electrodes. The electrode was prepared by casting the slurry containing 80 wt% of PHC-1, 10 wt% of super P, and 10 wt% of sodium alginate in deionized water onto copper foil and dried at 120 ^{o}C overnight. 1.0 M $NaPF_6$ in diethylene glycol dimethyl ether (diglyme) was used as the electrolyte and glass fiber (GF/D) was used as the separator. The mass loading of active materials was 1.0-1.5 mg cm^{-2}. The full cell was assembled using $Na_3V_2(PO_4)_3$ as the cathode material, PHC-1 as the anode material, and 1.0 M $NaPF_6$ in Diglyme as the electrolyte. The galvanostatic charge/discharge (GCD) and galvanostatic intermittent titration technique (GITT) test was performed on the LAND CT2001 battery tester. The voltage window is 0.01-2.5 V. Cyclic voltammetry (CV) and electrochemical impedance spectroscopy (EIS) were carried out on CHI600E electrochemical workstations.

The electrodes for in situ XRD and Raman were composed of 70 wt% of PHC-1 and 30 wt% of polytetrafluoroethylene (PTFE). The PHC-1 based electrode was discharged to 0.01 V and then charged to 2.5 V (in situ XRD at 50 mA g^{-1}; in situ Raman at 100 mA g^{-1}).

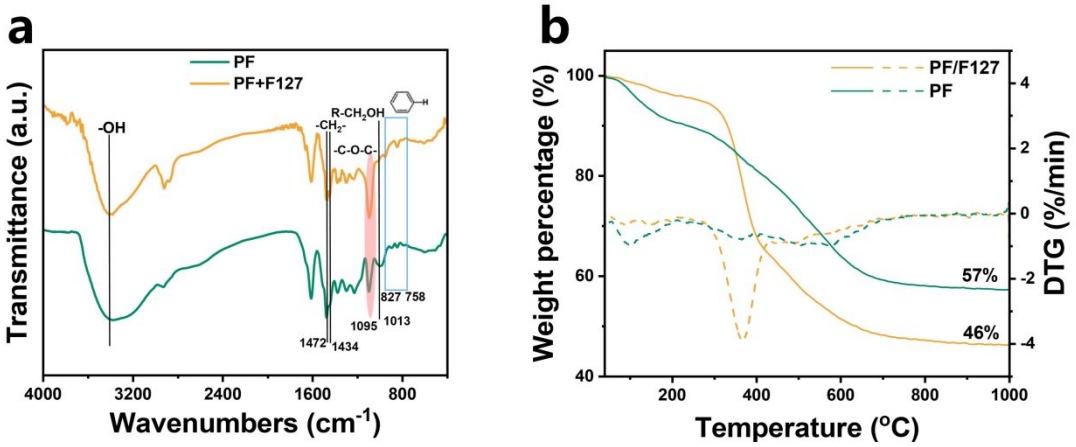

Figure S1. (a) FTIR spectra of phenol-formaldehyde (PF) resin and PF/F127 composite. (b) TGA-DTG curves of PF and PF/F127 composite.

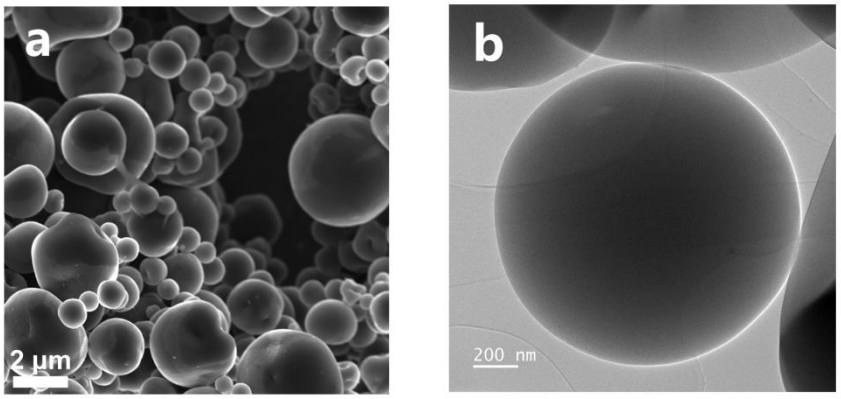

Figure S2. SEM (a) and TEM (b) images of PHC-0.

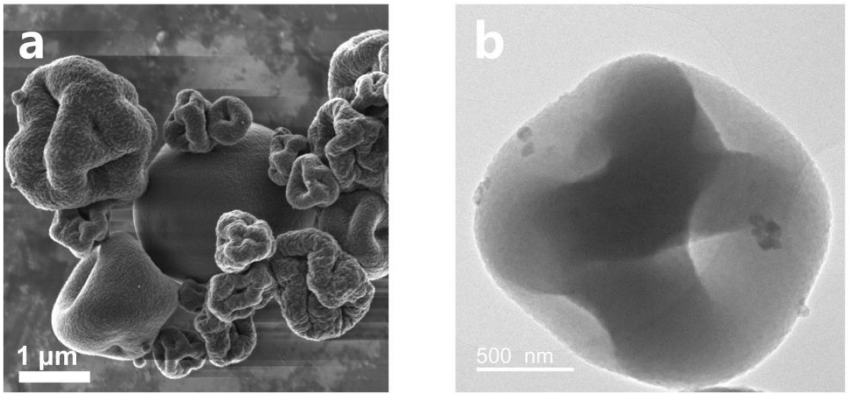

Figure S3. SEM (a) and TEM (b) images of PHC-2.

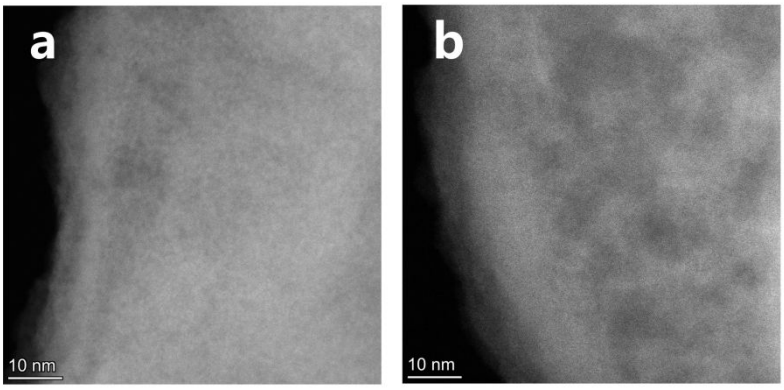

Figure S4. HAADF-STEM images of PHC-0 (a) and PHC-2 (b).

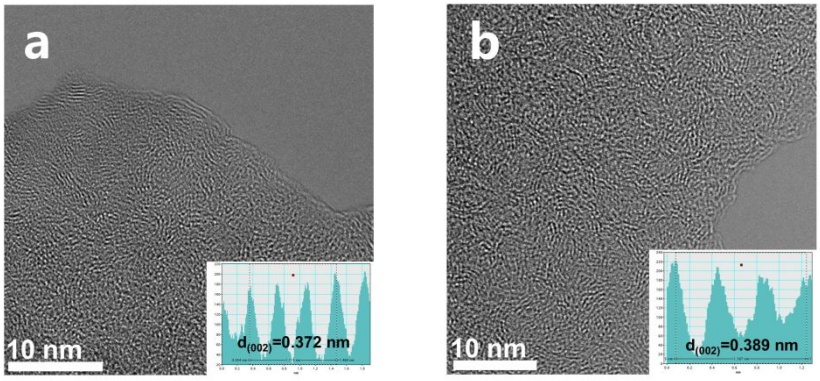

Figure 5. HRTEM images of PHC-0 (a) and PHC-2 (b).

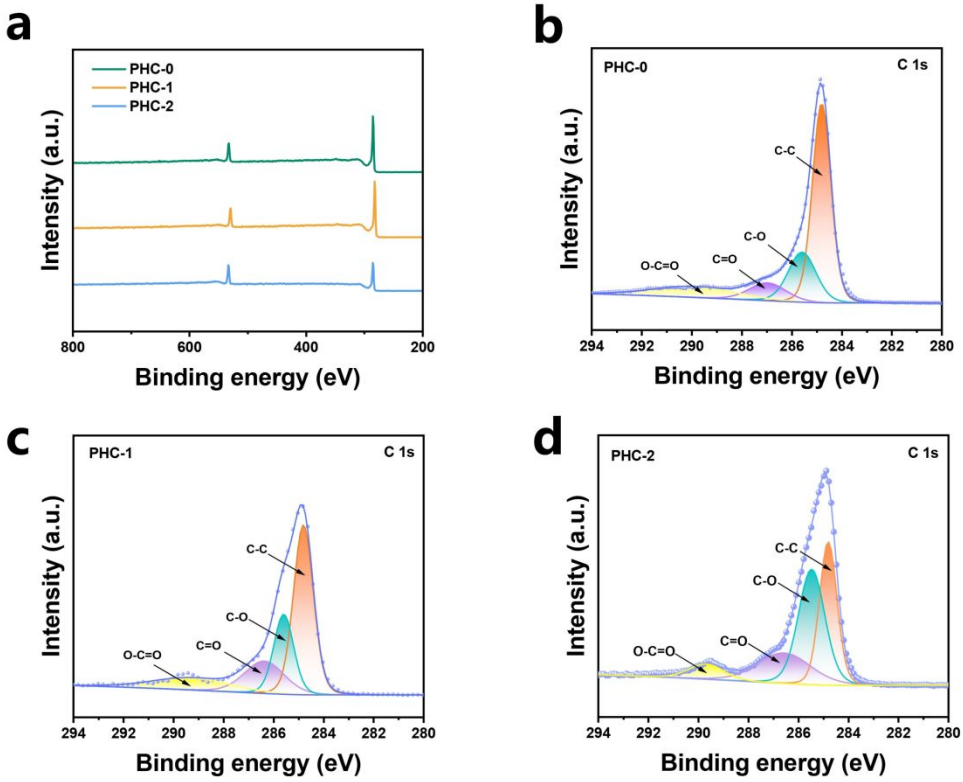

Figure S6. XPS characterization. (a) XPS survey spectra; (b-d) high-resolution C 1s XPS spectra for PHC-0, PHC-1, and PHC-2.

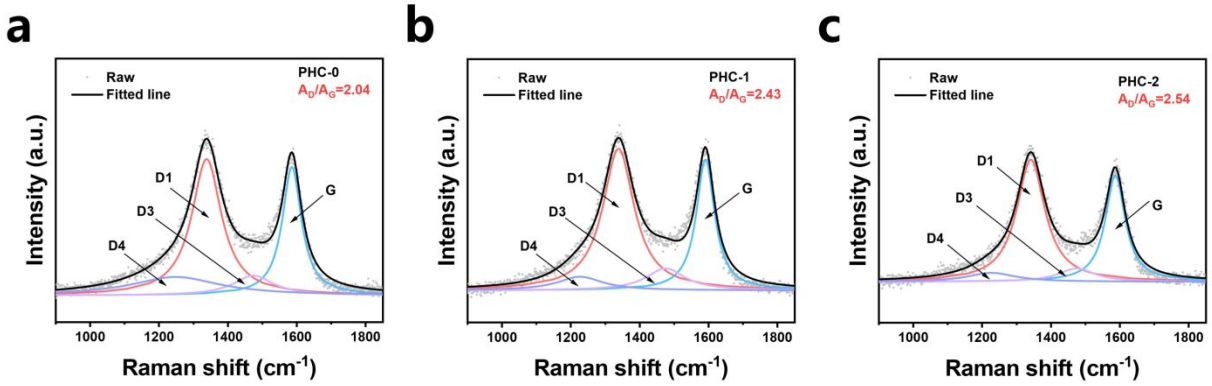

Figure S7. Raman spectra of (a) PHC-0, (b) PHC-1, and (c) PHC-2.

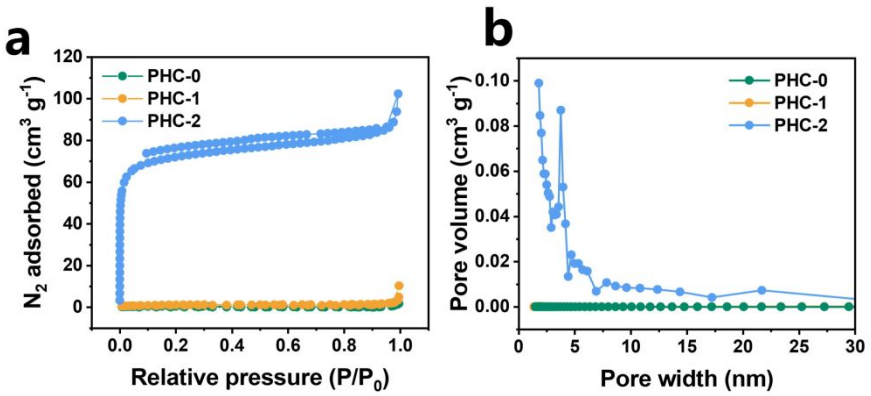

Figure S8. (a) N_2 adsorption-desorption isotherms and (b) the corresponding pore-size distribution of PHC-0, PHC-1, and PHC-2.

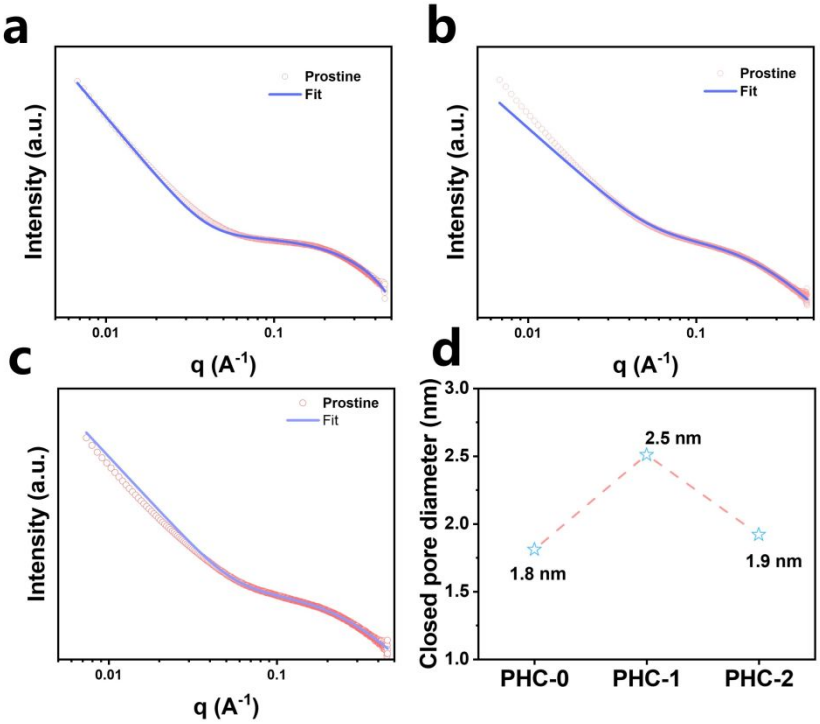

Figure S9. Fitted SXAS patterns. (a) SXAS patterns of PHC-0; (b) SXAS patterns of PHC-1; (c) SXAS patterns of PHC-2; (d) closed pore diameter of PHC-0, PHC-2, and PHC-1.

The patterns are fitted based on the following model: [1]

$$I(q) = \frac{A}{q^a} + \frac{Ba_1^4}{(1 + a_1^2 q^2)^2} + D$$

where q is the scattering vector, A and B are proportional to the total surface areas of the large and small pores, and D is a constant background term. The radius of closed nanopores can be obtained from the following formula:

$$R = 2 * a_1 * 10^{1/2}$$

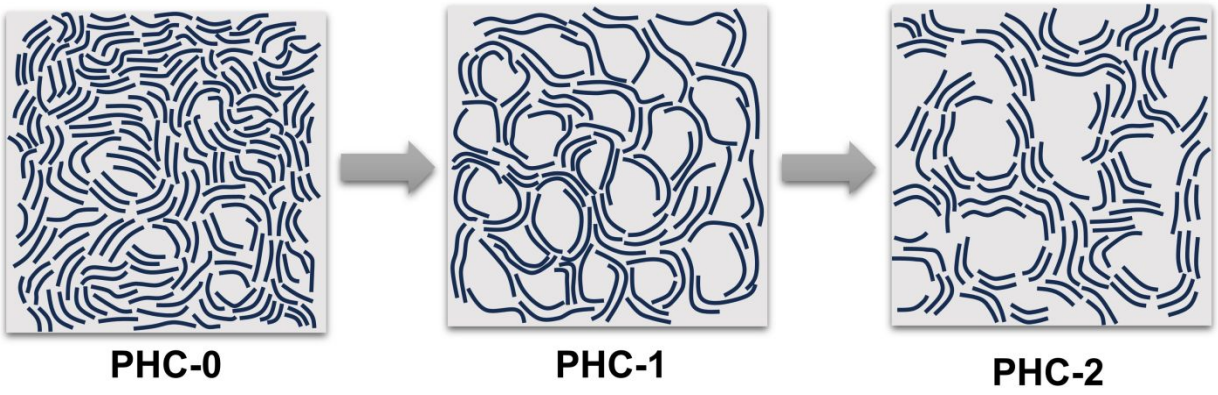

Figure S10. Schematic illustration of the pore structures of PHC-0, PHC-1, and PHC-2.

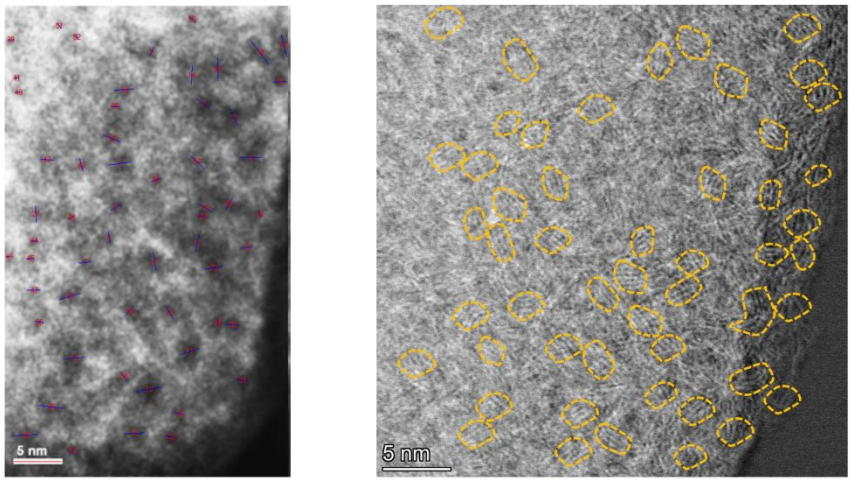

Figure S11. Statistical charts of PHC-1.

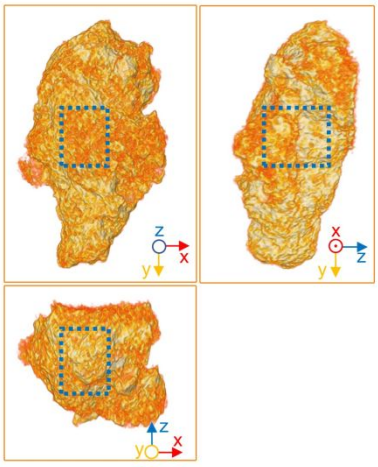

Figure S12. The reconstructed PHC-1 model at front, top, and right views.

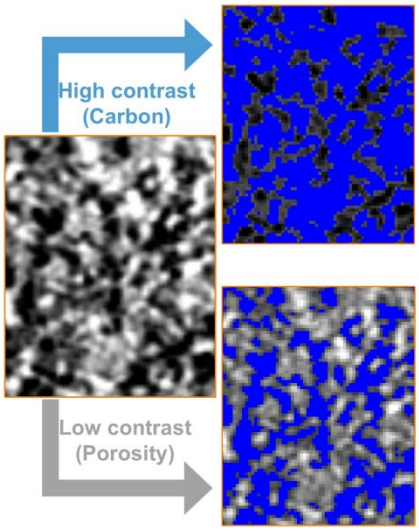

Figure S13. Illustration of the volume segmentation by contrast (Selected volume in orthoslice is filled by blue color).

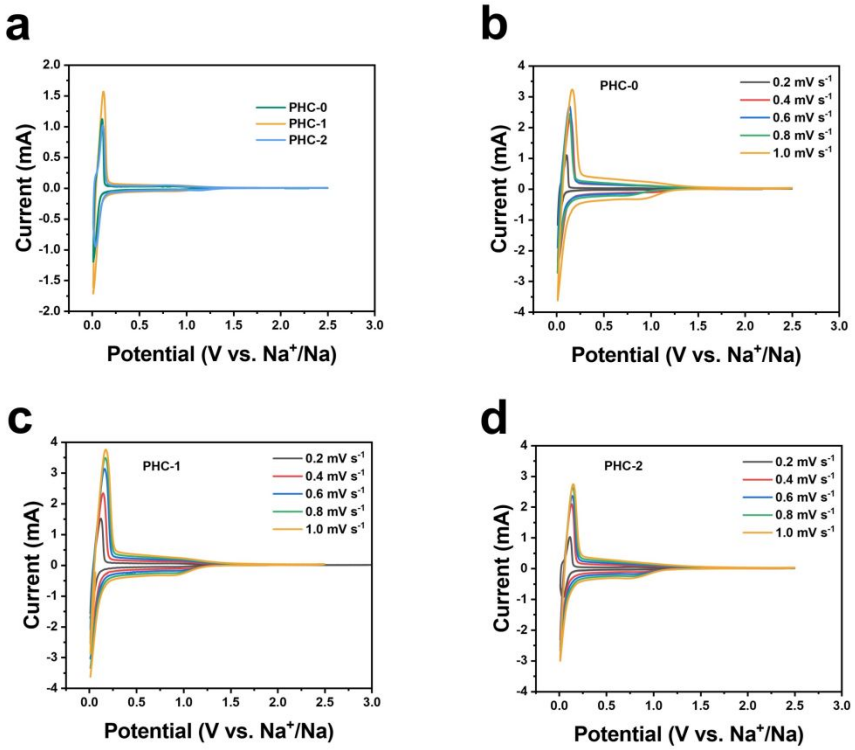

Figure S14. (a) CV profiles of the PHC-0, PHC-1 and PHC-2 at a scan rate of 0.2 mV s^{-1}. CV profiles of the (b) PHC-0, (c) PHC-1, and (d) PHC-2 at different scan rates.

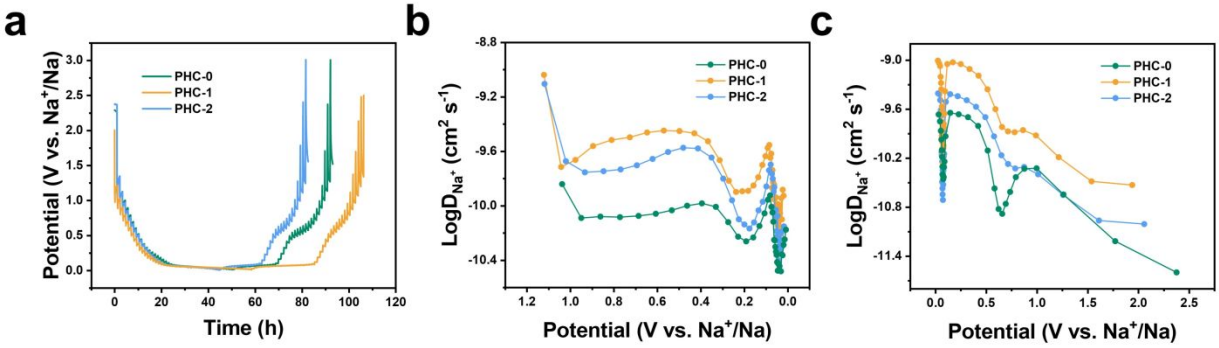

Figure S15. GITT curves (a) and calculated sodium-ion diffusion coefficients of PHC-0, PHC-1, and PHC-2 at (b) sodiation and (c) de-sodiation process.

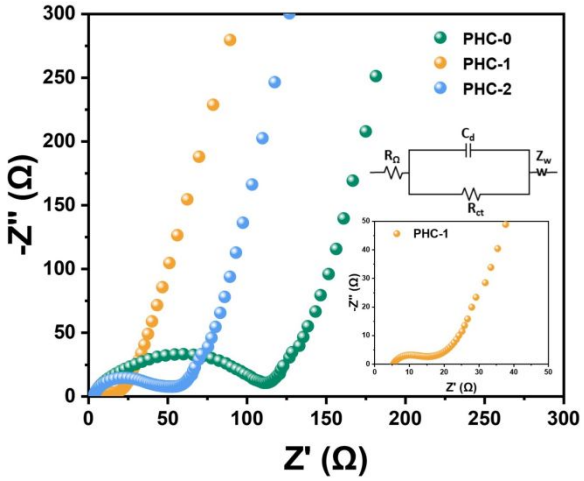

Figure S16. Electrochemical impedance spectroscopy (EIS) of PHC-0, PHC-1, and PHC-2. Insets are the zoomed view of EIS curve of PHC-1 and the equivalent circuit diagram.

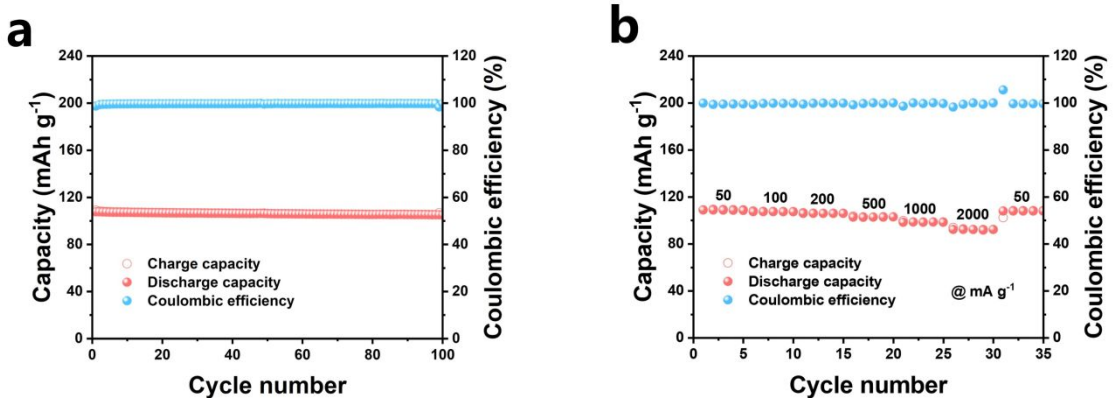

Figure S17. (a) Cycling performance at 50 mA g^{-1} and (b) rate performance of $Na_3V_2(PO_4)_3$.

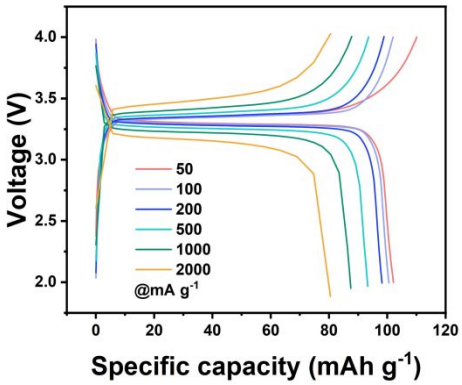

Figure S18. GCD curves at different current densities of the NVP//PHC-1 full cell.

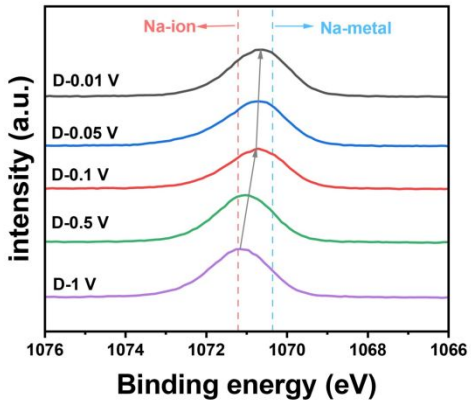

Figure S19. High-resolution Na 1*s* of PHC-1 at different potentials.

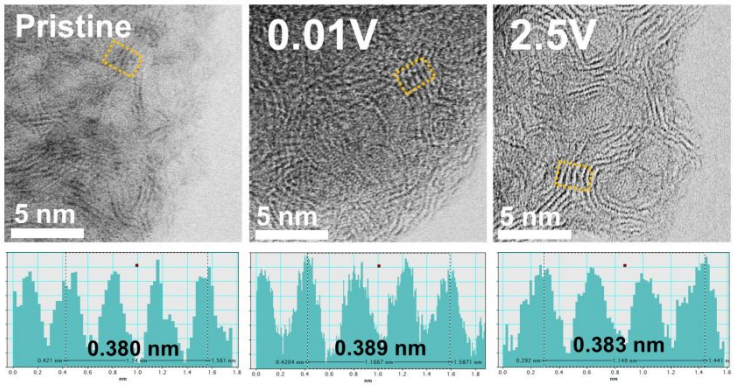

Figure S20. The interlayer spacing corresponding to the initial state, discharged to 0.01 V, and charged to 2.5 V.

Table S1. CHONS results of PHC-0, PHC-1 and PHC-2

Sample name	N (%)	C (%)	H (%)	S (%)	O (%)
PHC-0	0.12	94.16	0.56	0	5.16
PHC-1	0.14	91.47	0.60	0	7.79
PHC-2	0.08	89.95	0.60	0	9.39

(1) Zheng, Z.; Hu, S.; Yin, W.; Peng, J.; Wang, R.; Jin, J.; He, B.; Gong, Y.; Wang, H.; Fan, H. J., CO2-Etching Creates Abundant Closed Pores in Hard Carbon for High-Plateau-Capacity Sodium Storage. *Adv. Energy Mater.* 2024, *14* (3), 2303064.